

Physicochemical Characterisation and Histological Evaluation of Astaxanthin-loaded Nanoemulgel

Muhammad Syafiq Syamsul¹, Nuriana Munirah Hairul¹, Nor Khaizan Anuar¹ and Salizatul Ilyana Ibrahim^{1,2*}

¹Faculty of Pharmacy, Universiti Teknologi MARA, Cawangan Selangor, Puncak Alam Campus, 42300 Puncak Alam, Selangor, Malaysia

²Centre of Foundation Studies, Universiti Teknologi MARA, Cawangan Selangor, Dengkil Campus, 43800 Dengkil, Selangor, Malaysia

*Corresponding author (e-mail: saliza2910@uitm.edu.my)

Astaxanthin (AST), a lipophilic ketocarotenoid derived from seafood and microalgae, exhibits notable potential for skin health and ultraviolet (UV) protection. Its antioxidant properties effectively combat reactive oxygen species (ROS) within the skin layers. However, the oral bioavailability of AST is limited due to its lipophilic nature and poor water solubility. When applied topically, the antioxidant capabilities of AST can counteract oxidative stress and inflammation, contributing to its anti-ageing effects. Nevertheless, penetrating through the stratum corneum remains a challenge. To overcome this, nanoemulsion (NE) and nanoemulgel (NEG) have emerged as promising vehicles for enhancing AST delivery to the skin. This study characterised NE and NEG made from medium-chain triglyceride (MCT) oil and palm kernel oil (PKOlein) by particle size, polydispersity index (PDI), zeta potential, and pH. The mixed oil (MCT and PKOlein at a 1:1 ratio) NE had a smaller particle size (19.18 nm) and better stability (-27.14 mV zeta potential) than the MCT oil NE. However, the NEG formulations showed increased particle sizes, with MCT oil NEG exhibiting better stability (-11.47 mV) than the mixed oil variant. Solubility studies revealed that Tween 80-enhanced formulations significantly improved AST solubility, with phosphate buffer solution (PBS): Tween 80 (98:2) showing the highest solubility (13.255%). Meanwhile, histological studies demonstrated superior skin permeation for MCT oil formulations, attributed to shorter fatty acid chains, while mixed oil formulations exhibited better retention in the dermis layer. In conclusion, MCT oil offers better skin permeation, whereas mixed oil formulations provide sustained dermal retention, suggesting their potential for various topical applications. This research highlights the advantages of using MCT and mixed oil formulations to enhance the delivery and efficacy of active compounds in skincare products.

Keywords: Antioxidant; astaxanthin; medium-chain triglycerides oil; nanoemulgel; transdermal delivery

Received: September 2024; Accepted: January 2025

The skin, the body's largest organ, has a pH of 4.1 to 5.8 and serves as a barrier against environmental hazards [1]. Ageing, accelerated by UV radiation (photoaging), leads to cellular changes like genomic instability and mitochondrial dysfunction, characterised by wrinkles, dryness, and pigmentation [2]. Free radicals, reactive molecules with unpaired electrons, cause oxidative stress by stealing electrons from other molecules [3].

Antioxidants neutralise oxidative damage, with AST being a potent antioxidant, surpassing vitamins C and E in strength. AST is a ketocarotenoid that can be sourced and isolated from various seafood, including salmon, shrimp, and the microalgae *Haematococcus pluvialis*. Extensive research has explored its potential benefits for skin health and UV protection. When applied topically, AST counteracts oxidative stress and inflammation contributing to its anti-ageing

properties (4). When applied topically, AST counteracts oxidative stress and inflammation contributing to its anti-ageing properties (4). However, traditional topical formulations incorporating antioxidants struggle with poor drug penetration due to the stratum corneum barrier and drug properties like high melting points or hydrophilicity [6].

Nanoemulsion (NE), using medium-chain triglycerides (MCTs) as the lipid carrier, offers a solution by enhancing aqueous solubility, stability, and biological activity [7]. Characterised by oil droplets with a diameter below 200 nm, NEs are formed by blending immiscible phases like oil and water, stabilised by surfactants like Tween 80 [8]. NEs improve cutaneous permeation and encapsulate higher concentrations of active compounds, but their low viscosity and rapid drug release limit their topical application [9]. Non-ionic surfactants such as Tween

80 are preferred for their reduced irritation and skin compatibility [10]. Nanoemulgels (NEGs), derived from NEs, combine the benefits of nanoemulsions and hydrogels to improve skin retention and drug delivery [11]. Their small size facilitates efficient crossing of biological barriers, which include the tight junctions of the blood-brain barrier. This characteristic enhances cellular uptake and permeation, making nanogels promising candidates for targeted drug delivery systems and other biomedical interventions [12]. NE-based nanogels leverage the advantages of NEs to optimise hydrophobic drug delivery. Their small size and high viscosity improve topical application and stability, addressing the limitations of conventional formulations [13].

This study aims to formulate AST-loaded NEs and NEGs using fractionated medium-chain triglycerides (FMCTs) as well as assess their physicochemical properties and skin permeation profiles via *ex vivo* rat skin studies. MCTs are derived from palm tree *Elaeis guineensis* through a refining process that yields crude palm oil (CPO) and palm kernel oil (PKO) [14]. MCTs oil typically comprise a blend of triacylglycerols that are rich in saturated medium-chain fatty acids, specifically C_{8:0} and C_{10:0}. Meanwhile, MCTs or FMCTs are produced through the fractionation of palm kernel olein [15]. The fatty acid composition of palm kernel olein (PKOlein) is dominated by lauric acid (C_{12:0}), which makes up 46%. Fatty acids are categorised based on carbon chain length, with 1 to 11 carbon chains considered as short-chain triglycerides (SCTs), 7 to 12 carbon chains termed MCTs, and more than thirteen carbon chains classified as long-chain triglycerides (LCTs) [14].

Franz diffusion cells were employed to evaluate the formulation's permeation, a widely recognised tool in dermatopharmacokinetics. This system consists of two compartments; the donor compartment, where the test formulation is applied with the stratum corneum facing it, and the receptor compartment, which contains a buffered receptor fluid emulating a physiological condition. The receptor fluid maintains a constant temperature and pH to ensure experimental consistency. The Franz diffusion cell method is advantageous due to its minimal sample requirement, making it suitable for expensive or limited-availability compounds [16]. Histological evaluation using Oil Red O (ORO) staining was conducted to assess formulation penetration. ORO stains lipophilic components and allows tracking of lipid accumulation within the skin. Before staining, the skin's natural lipids were removed to prevent interference, ensuring the results reflected only the applied formulation. This method provides accurate visualisation of lipid penetration and accumulation within the skin [17].

This approach aims to improve antioxidant delivery through topical nanocarriers like nanoemulsions (NE) and nanoemulsion gels (NEG), which enhance encapsulation and skin penetration of lipophilic

ingredients like astaxanthin (AST). These formulations aim to improve skin health by addressing ageing signs and dermatological disorders. The findings contribute to advancing NE and NEG formulations for skincare, offering enhanced delivery and efficacy.

EXPERIMENTAL

Chemicals and Materials

Astaxanthin was obtained from Astareal®, United States of America. Tween 80, Tween 85, and Carbopol 940 were purchased from Sigma-Aldrich, USA. Standard fatty acid methyl ester mixture (FAME) was purchased from Sigma-Aldrich (St. Louis, USA). PKO, PKOlein, and MCT oils were supplied by the Malaysian Palm Oil Board (MPOB). Standard triglycerides (TG mixture (tricaprylin, tricaprillin, trilaurin, trimyristin, tripalmitin, and triolein) were purchased from Sigma-Aldrich (St. Louis, USA). The silylating reagent of N, O-Bis (Trimethylsilyl) trifluoroacetamide with 1% trimethylsilyl chloride (BTSA) were purchased from Fluka Chemicals (Buchs, Switzerland). Dimethylformamide (DMF) and dichloromethane (DCM) were purchased from Mallinckrodt Baker Inc., Phillipsburg, New Jersey, USA. The Oil Red O Stain Kit (ScyTek Laboratories, USA), Harris hematoxylin (VWR International, UK), and eosin (Microm International, Germany) were used in histology examination. All the chemicals are of analytical grade and were directly used without further purification.

Determination of Fatty Acids and Triglycerides Composition Using Gas Chromatography Analysis

The study employed gas chromatography (GC) to analyse the fatty acid composition of PKO, PKOlein, MCT oil, and a 1:1 mixture of MCT oil and PKOlein. The oils were first converted into FAME by base-catalysed, as described by Japir et al. [18].

The GC analysis was performed using an Agilent model 7890B system with a flame ionisation detector (FID) and a fused-silica capillary column (BPX 70) of precise size and specifications. Helium was used as the carrier gas. The temperature programming for the column, injector port, and detector, as well as the split ratio, follows the requirements provided by Bahadi et al. [19]. Peaks were identified by injecting the appropriate FAME into the GC instrument and comparing 17 of them to FAME standards, analysed under identical conditions. This was followed by quantifying individual fatty acids using retention durations.

The analysis of triglycerides (TGs) composition in oils using an Agilent model 7890B GC equipment outfitted with a flame ionisation detector (FID) as well as a split and a splitless injection port. A polyimide-coated fused silica capillary column ZB-5HT Inferno (15 m length x 0.53 mm internal diameter) with a film

thickness of 0.15 μm was used in this analysis. The GC system's column flow was helium (He) at 5 mL/min, while the flame FID system used hydrogen (H_2) at 30 mL/min and oxygen (O_2) at 400 mL/min. The split ratio was adjusted to 100:1, with the inlet temperature retained at 280°C.

The GC temperature programme featured a detector temperature of 300°C. The oven temperature started at 80°C with no hold time and ramped up at the rate of 5°C per minute until 250°C, where it was kept for 16 minutes. To prepare the standards and oils, approximately 0.01 g of each sample was weighed and placed into a 5 mL vial. Then, 0.5 mL of DMF, 0.5 mL of DCM, and 0.2 mL of BTSFA were pipetted into the vial with the samples. The vial was tightly sealed and homogenised with a vortex mixer. The sample vial was placed in a water bath and heated to 60°C for 30 minutes. Following cooling, the mixtures were transported to the GC. The TG compositions of each oil (reported as relative percentages) were derived from the GC's peak regions, which corresponded to retention times relative to standards analysed under identical conditions [20].

Formulation of Nanoemulsion and Nanoemulgel

AST NEs were made through spontaneous emulsification method, which is also known as the low-energy method due to its simple implementation, low cost, and high energy efficiency [21]. This technique required the combination of oil, surfactant, and water with a ratio of 3:25:72 respectively, under carefully controlled conditions, where the Gibbs free energy of emulsification is inherently lower than zero. This refined process ensures the creation of NE with enhanced stability and optimal AST formulation [22]. Due to the rapid diffusion of the surfactant from the oil phase into the aqueous phase, the emulsions formed spontaneously when the oil phase was combined with the aqueous phase [21]. The organic phase comprises MCT oil, bioactive AST, and hydrophilic nonionic surfactant blend (Tween 80 and Tween 85 in a 2:1 ratio). Under magnetic stirring, the aqueous (deionised water) phase was meticulously introduced drop by drop into this combination. This controlled process ensures gradual and uniform creation of oil-in-water NEs to yield finely dispersed nanodroplets. NEs were stored in aluminium-covered glass containers in a dark environment to guarantee the utmost stability and preservation of bioactivity.

Hydrogel was prepared by introducing water to Carbopol 940, followed by homogenisation to attain uniform dispersion. To adjust the pH of the hydrogel, a few drops of Triethanolamine (TEA) were added under continuous stirring. The mixture was continuously stirred for 24 hours to facilitate the gelation process. Subsequently, the optimised

formulation of AST-loaded NE was incorporated into the Carbopol 940 hydrogel with a ratio of 3:1. This method ensures a precisely controlled and homogenous hydrogel system for the encapsulation and delivery of the AST-loaded NE [23].

Characterisation of Nanoemulsion and Nanoemulgel

The zeta potential of NEs was determined using a Zetasizer nano ZS® (Malvern Instruments, UK) in electrophoretic mode, employing a laser with a wavelength of 633 nm, at an angle of 175°, and a temperature of 25 °C. Triplicate measurements for each parameter were done, with zeta potential (ZP) values falling within the +100 to -100 mV range. Colloidal stability predictions were made based on ZP magnitude, where values exceeding +25 mV or falling below -25 mV indicate a high degree of stability. Conversely, lower ZP values suggested potential for aggregation, coagulation, or flocculation due to van der Waals interparticle attraction [9, 24]. Particle size analysis was performed on dried samples dispersed in distilled water using a Malvern Zetasizer nano ZS® (Malvern Instruments, UK). The settings included a particle 20 refractive index of 1.9, a particle absorption index of 0.01, a water refractive index of 1.33, and a laser obscuration of 12% [22]. Furthermore, the pH of each NE sample was measured at 25 °C using a digital pH meter (Mettler Toledo Seven Multi, Greifensee, Switzerland) equipped with a glass electrode. Thirty millilitres of each sample were utilised and three pH readings were recorded to assess the acidity or alkalinity of the NEs [25].

In Vitro Skin Permeation Study of Astaxanthin Nanoemulsion and Nanoemulgel

Solubility Studies of Astaxanthin in Various Medium

The solubility of AST in various solvents and co-solvents was determined using a UV-Vis spectrophotometer (Thermo Fisher/Genesys 180, UK) to select the optimal receptor medium for the *in vitro* analysis. The receptor mediums were prepared in several concentrations with different combinations of diluents as shown in Table 1. In each receptor medium, 10mg of pure AST was diluted in either ethanol (EtOH), Tween 80 (in the absence of EtOH), or directly in PBS (in the absence of EtOH and Tween 80).

Before the sampling started, the samples were incubated in the water bath with a shaker for 72 hours and were centrifuged at 3500 rpm for 30 minutes using a benchtop centrifuge (Labofuge 200, Germany). This method was adapted from Khalid et al. [26]. To determine the solubility of AST, the lower aqueous phase was filtered by a 0.45 μm nylon syringe filter and quantified.

Table 1. Receptor medium and the ratio for each combination.

Receptor Medium	Ratio
EtOH	1
PBS	1
PBS: EtOH	80:20
PBS: Tween 80	98:2
PBS: Tween 80: EtOH	79:1:20
PBS: Tween 80: EtOH	73:2:25

EtOH: Ethanol, PBS: Phosphate Buffer Solution pH 7.4

In Vitro Skin Permeation Study

Seven male Wistar rats, aged between 9 to 10 weeks, were used in this research. The rats were sourced from the Laboratory Animal Facility and Management (LAFAM) after obtaining the approval from the UiTM Ethics Committee on Animal Research and Ethics (UiTM CARE). The animals were euthanised using carbon dioxide (CO₂) inhalation. After confirming respiratory cessation, the ventral region of the rat was shaved using an electronic shaver and razor blade. Circular skin sections (approximately 3 cm in diameter) were excised and any residual subcutaneous fat, blood vessels, and connected tissue were cleared. The skin treated was then cleaned with normal saline. The skin pieces were rinsed with normal saline, wrapped in aluminium foil, and stored at - 20°C to preserve the skin viability and permeability till usage (up to one month) [27]. The skin was pre-hydrated with phosphate buffer solution (pH 7.4) for 30 minutes before mounting it between the donor and receptor chambers of Franz diffusion cells. The stratum corneum faced the donor chamber, while the dermal side faced the receptor chamber. Initially, the receptor chamber contained phosphate buffer saline-Tween 80 mixture (98:2) as the receiving medium and was stirred continuously at 100 rpm at a temperature of 32± 0.5 °C [28]. The organic solvent was introduced into the receptor fluids to promote drug solubilisation and ease its chemical assay [29,30]. The donor chamber remained empty for the first 30 minutes. As shown in Table 2, 1 g of each formulation (containing 300 µg of AST) was applied to the skin's surface in the donor chambers (except the control), which were then sealed and incubated for 24 hours.

Histological Evaluation

Following the diffusion study, the skin was washed with normal saline. Subsequently, the control group underwent formalin fixation, dehydrated using a graded series of alcohols, embedded in paraffin wax, and microtomed. The skin was then subjected to the hematoxylin and eosin staining procedure. As for the treatment group, a cryostat (CM1850UV-1-1, Leica, Germany) was used to segment skin perpendicularly at a 90° angle to the epidermal surfaces to get full-thickness skin, with a thickness of 5 µm. There were several steps for staining as instructed in the ORO kit obtained from ScyTek. The Oil Red O staining procedure began with heating the Oil Red O Solution to 60°C. Fresh or frozen tissue sections were prepared as usual. Slides were then placed in propylene glycol at room temperature for 5 minutes. Following this, the slides were incubated in the heated (60°C) Oil Red O Solution for 6-10 minutes or overnight at room temperature. A mixture of 85% propylene glycol in distilled water was prepared. Tissue sections were differentiated in 85% propylene glycol for 1 minute. The slides were rinsed in two changes of distilled water. The tissue sections were stained with Hematoxylin, Mayer's (Lillie's Modification) for 1-2 minutes. The slides were thoroughly rinsed in tap water, followed by two changes of distilled water. Finally, the slides were covered with a slip using an aqueous mounting medium (cat# AML060) [27]. Microscopic examination allowed for the assessment of alterations in skin structure and elastosis by viewing under a compound binocular microscope (Leica CME 1349522X, Leica, Germany) at a magnification level of 40x compared with the control sample [31].

Table 2. Formulation treatment groups for in vitro skin permeation and histological study.

Group	Rat(s)	Formulation
Untreated	1	Normal saline solution (control)
Treated	2	AST NE using MCTs oil
	3	AST NE using MCTs: PK Olein oil (1:1)
	4	AST NEG using MCTs oil
	5	AST NEG using MCTs: PK Olein oil (1:1)

AST: Astaxanthin, NE: Nanoemulsion, NEG: Nanoemulge

RESULTS AND DISCUSSION

Fatty Acid and Triglycerides Composition using Gas Chromatography (GC) Analysis

MCTs have been extensively studied for their diverse benefits in human metabolism, physiological responses, nutrition, and pharmaceutical applications [31]. Table 3 highlights the distinct profiles of caprylic, capric, and lauric acids in PKO, PKOlein, MCT oil, and a blend of MCT and PKOlein. PKO shows a moderate presence of a high concentration of lauric acid (46.0%). This high lauric acid content contributes to PKO's use in soap and cosmetic production due to its strong antimicrobial properties [32]. PKOlein, a fractionated version of PKO, slightly increases the content of caprylic (3.4%) and capric acids (3.2%), while significantly reducing lauric acid to 13.8%. This alteration makes PKOlein more

suitable for applications as it requires a lower melting point and improves oxidative stability such as in cooking oils [33]. Notably, MCT oil stands out with exceptionally high concentrations of caprylic (55.8%) and capric acids (44.0%), with no detectable lauric acid. This composition makes MCT oil highly valued in the health and nutrition sector, particularly for its moisturising and quick absorption properties [34]. The mixture of MCT and PKOlein combines the characteristics of both oils, which show intermediate levels of caprylic acid (25.81%), capric acid (21.68%), and lauric acid (23.56%). This mixture harnesses the benefits of both components, which offer a balanced profile that can be advantageous in various formulations. Moreover, the mixture facilitates the rapid absorption of MCTs. With the functional properties of PKOlein that are more thermostable, it is more versatile for use in topical applications cosmetics, and food products [34].

Table 3. Fatty Acid composition using gas chromatography.

Fatty Acid Composition ^a	PKO	PKOlein	MCT	MCT: PKOlein (1:1)
Cy (C _{8:0})	2.9%	3.4%	55.8%	25.81%
C (C _{10:0})	3.0%	3.2%	44.0%	21.68%
La (C _{12:0})	46.0%	13.8%	Not detected	23.56%

^aLetters in parenthesis indicate abbreviation for corresponding fatty acid: Cy, caprylic acid; C, capric acid; La, lauric acid

Table 4. Triglycerides composition using gas chromatography.

ECN ^a	Expected TG ^b	Name	PKO	PKOlein	MCT	MCT: PKOlein (1:1)
24	CyCyCy	Tricaprylin	ND	0.37%	23.42%	12.01%
26	CyCCy	Dicaprylin-monocaprin	ND	0.86%	43.33%	22.17%
28	CCyC	Dicaprin-monocaprylin	ND	0.83%	26.55%	13.66%
30	CyCLa	Caprylin-caprin-laurin	1.17%	1.52%	5.49%	3.49%
32	LaCyLa	Dilaurin-monocaprylin	6.28%	7.29%	0.11%	3.71%
34	LaCLa/MCyLa	Dilaurin-monocaprin/myristin-caprylin-laurin	8.52%	9.17%	ND	4.63%

^aECN, Equivalent Carbon Number; value in parenthesis indicates the number of double bonds in the TG.

^bLetters in parenthesis indicate abbreviation for corresponding fatty acid: Cy, caprylic acid; C, capric acid; La, lauric acid; M, myristic acid.

Analysing triglyceride (TG) composition is crucial for evaluating the purity of oils and identifying specific TGs in each sample, ensuring the results accurately reflect the true composition without impurities. Gas chromatography (GC) is widely employed for this purpose due to its speed, convenience, and sensitivity (35). The fatty acids in triglycerides can mimic natural skin lipids, making them effective for restoring the skin barrier function. This is especially important for ageing or damaged skin, where lipid levels may be depleted (36). Caprylic/Capric Triglyceride is commonly used as an emollient, penetration enhancer, drug carrier, and solvent in oral and dermal formulations. Table 4 shows that MCT oil contains the highest amount of tricaprylin (23.42%). However, the mixture of MCT: PKOlein (1:1) exhibits the most balanced composition of tricaprylin, dicaprylin-monocaprin, and dicaprin-monocaprylin, indicating a stable profile across ECNs 24, 26, and 28 (37).

Characterisation of Nanoemulsion and Nanoemulgel

Table 5 presents the detailed characteristics of NE and NEG formulations, which include MCT oil and a mixed oil blend. The table details the particle size, polydispersity index (PDI), zeta potential, and the pH of these formulations.

The particle sizes range from 19.18 nm to 189.53 nm. The mixed oil NE exhibits a smaller average particle size of 19.180 ± 0.526 nm compared to the MCT oil NE (26.353 ± 4.322 nm). This smaller particle size in the mixed oil NE is advantageous because smaller particles can penetrate deeper into the skin, enhancing the delivery of active ingredients into the dermal layers. In contrast, the larger particles in the MCT oil NE may not permeate as effectively, primarily remaining along the hair follicles [35]. In the NEG formulations, the particle size increases, with MCT oils at 80.717 ± 34.274 nm and mixed oil at 189.533 ± 50.677 nm, indicating potential aggregation in the gel matrix [36]. However, all formulations still

have particle sizes below 200 nm, qualifying them as nanoparticles and making them suitable for skin penetration.

The polydispersity index (PDI), which measures the uniformity of particle size distribution, ranges between 0.321 and 0.438. The lowest PDI value is 0.321 ± 0.139 for the MCT oil NE, followed by 0.349 ± 0.032 for the mixed oil NE. Both values are below 0.4, indicating a narrow size distribution and a monodispersed system [37]. This indicates that the particle size distribution is almost uniform and homogeneous throughout the formulation [38]. In the NEG formulations, the PDI for MCT oils is 0.438 ± 0.183 . This is 0.358 ± 0.033 for the mixed oil, which shows a broader size distribution. These PDI values indicate that the NEG, especially MCT oil NEG which exhibits polydispersity, could potentially lead to instability over time [36].

The zeta potential, an indicator of the stability of colloidal dispersions, is significantly higher in the mixed oil NE (-27.14 ± 4.750 mV) compared to the MCT oil NE (-8.437 ± 4.668 mV). A higher absolute zeta potential value indicates greater stability by increasing electrostatic repulsion between particles, reducing the likelihood of aggregation. This repulsion prevents particles from clumping together to maintain a uniformly dispersed system, which is essential for the stability and effectiveness of the formulation [39]. Thus, the mixed oil NE is likely more stable than the MCT oil NE. The zeta potential for the MCT oil NEG is -11.47 ± 1.374 mV, indicating a slightly greater stability than the mixed oil NEG at -7.467 ± 1.174 mV. Zeta potential measures the electrical charge on the surface of nanoparticles in a dispersion. Lower zeta potential suggests a higher chance of particles settling out or aggregating, leading to reduced stability and uniformity of the formulation [40]. Based on this, the NEG, particularly mixed oil NEG, has a higher tendency to aggregate and is less stable compared to other formulations.

Table 5. Characterisation of astaxanthin NE and NEG.

Type of Formulation	Particle Size (nm)*	PDI*	Zeta Potential (mV)*	pH*
MCT oils NE	26.353 ± 4.322	0.321 ± 0.139	-8.437 ± 4.668	6.546 ± 0.281
Mixed Oil NE	19.180 ± 0.526	0.349 ± 0.032	-27.14 ± 4.750	6.447 ± 0.052
MCT oils NEG	80.717 ± 34.274	0.438 ± 0.183	-11.47 ± 1.374	5.942 ± 0.130
Mixed Oil NEG	189.533 ± 50.677	0.358 ± 0.033	-7.467 ± 1.174	5.883 ± 0.093

MCT: Medium chain triglycerides, NE: Nanoemulsion, NEG: Nanoemulgel

*Value is expressed as Mean \pm SD

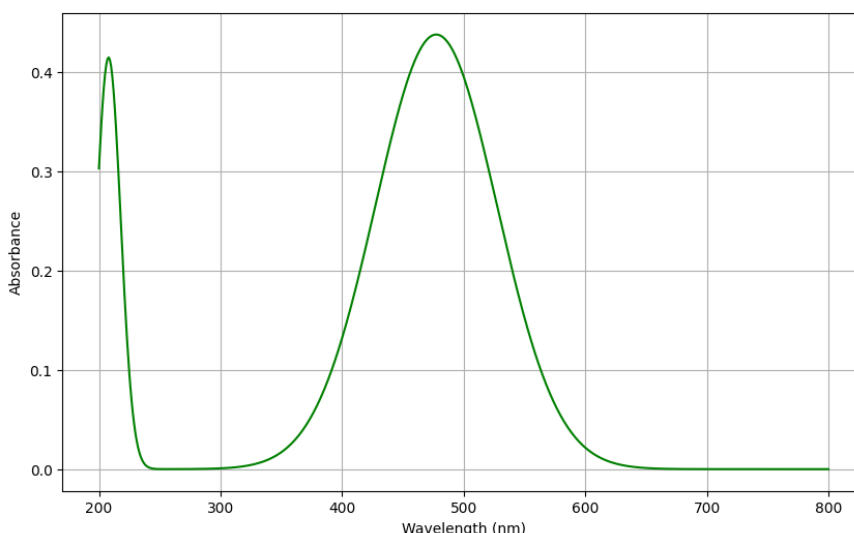


Figure 1. The wavelength of astaxanthin in pure ethanol.

Table 6. Concentration of AST against absorbance at 477.405 nm.

Concentration (ug/ml)	Absorbance (AU)
2	0.1061
4	0.198
6	0.3119
8	0.4067
10	0.495
12	0.6032

Additionally, the pH values of the formulations are close to the natural pH of human skin, which is around 5.5 to 6.5. The MCT oil NE has a pH of 6.546 ± 0.281 , while the mixed oil NE has a pH of 6.447 ± 0.052 . Both NEGs have slightly acidic pH values, with MCT oils at 5.942 ± 0.13 and mixed oil at 5.883 ± 0.093 , remaining within an acceptable range for skin application. Although the decrease in pH is attributed to the addition of Carbopol 940, it stays within the optimal pH range for human skin [41]. Maintaining a pH close to that of the skin is crucial to avoid irritation and ensure compatibility with the function of the skin's natural barrier [42].

Overall, the mixed oil NE demonstrates superior properties in particle size and zeta potential, suggesting enhanced stability and skin penetration compared to the MCT oil NE. However, in the NEG form, the MCT oil formulation shows slightly better stability and uniformity than the mixed oil NEG.

Solubility Studies of Astaxanthin in Various Medium

Determination of Absorbance Value

The AST solution, prepared at a concentration of 1 mg/mL in ethanol, was analysed using a UV-Vis spectrophotometer. The resulting UV-Vis spectrum

was examined to identify the wavelength corresponding to the maximum absorbance of AST. Based on the spectrum, the wavelength of 477.405 nm was selected for further analysis as it showed the highest peak area (Figure 1), which indicated the maximum absorbance for AST at this wavelength. This selection aligns with previous studies which suggested that the appropriate wavelength range for AST absorbance is between 430-550 nm [43]. Therefore, the wavelength of 477.405 nm was chosen as it falls within this range and represents the peak absorbance observed in the analysis.

Table 6 shows a positive correlation between absorbance and concentration at 477.405 nm. As concentration increased from 2 µg/mL to 12 µg/mL, absorbance values rose steadily from 0.1061 to 0.6032, indicating a linear relationship between concentration and absorbance within the measured range. These absorbance values were used to plot a graph of absorbance versus concentration, which yielded a linear relationship. The linear regression analysis of the calibration curve produced the equation $y = 0.0503x$, where y represents the absorbance, and x represents the concentration of AST. The coefficient of determination (R^2) value of 0.9987 indicates that 99.87% of the variability in absorbance can be explained by the linear relationship with concentration. This high R^2 value suggests that the calibration curve

is highly reliable and demonstrates excellent linearity over the tested concentration range. The calibration curve provides a reliable method for determining the concentration of AST in a sample based on its absorbance at 477.405 nm, enabling accurate quantification of AST in various formulations or samples [44].

Determination of Solubility Study

Table 7 shows the solubility of AST was highest in PBS: T80 (98:2), with 26.5100 µg (13.255%), and lowest in PBS alone, with 3.1601 µg (1.580%). The solubility study encompassed six different solvent mixtures, with solubility monitored via absorbance readings. PBS alone exhibited the lowest average solubility, with a solubility of 1.58% and an average concentration of 3.160 ± 0.001 µg. This low solubility is attributed to AST's hydrophobic properties, which favor solubility in organic solvents. In comparison, AST showed an average solubility of 21.907 ± 0.001 µg in ethanol, which corresponded to a solubility percentage of 10.95%. Despite AST's propensity for solubility in organic solvents, its solubility in ethanol remained relatively low at 0.038 g/L [45].

The solvent mixture that exhibited the highest average solubility was PBS: Tween 80 (98:2), with an average solubility of 26.51 ± 0.004 µg and a solubility percentage of 13.255%. This notable increase in solubility is likely attributable to the surfactant properties of Tween 80. Tween 80 works by encapsulating hydrophobic molecules to reduce surface tension between aqueous and non-aqueous

phases, ultimately increasing the solubility of the formulation [46]. Other combinations showed moderate average solubility: PBS: T80: EtOH (73:2:25) with an average solubility of 23.903 ± 0.001 µg, PBS: T80: EtOH (79:1:20) with an average solubility of 23.26 ± 0.001 µg, and PBS: EtOH (80:20) with an average solubility of 4.135 ± 0.001 µg. Other mixtures containing Tween 80 also showed an increase in average solubility, indicating that Tween 80 plays a crucial role in enhancing solubility. These results indicate that the presence of Tween 80, even in varying ratios, significantly enhances the solubility of AST. The moderate solubility in PBS: EtOH (80:20) also underscores the importance of Tween 80 in achieving a higher solubility level [47].

Histological Evaluation

Table 8 presents the permeability of different formulations on the skin. The skin sections (No. 1) were stained with Haematoxylin and Eosin (H&E) to show the physiological structure. The control ORO (No. 2) represents the skin stained with Oil Red O (ORO) without any formulation. Samples (No. 3) to (No. 6) contained the formulation and were stained with ORO.

The results obtained from the histology procedures for skin permeation were compared with the control ORO, which indicated the skin without any formulation added. The skin that was stained with H&E was used as the comparison of the normal skin physiology. H&E staining provides a clear contrast between different tissue compartments (layers) and depicts a detailed view of how the tissues are structured [48].

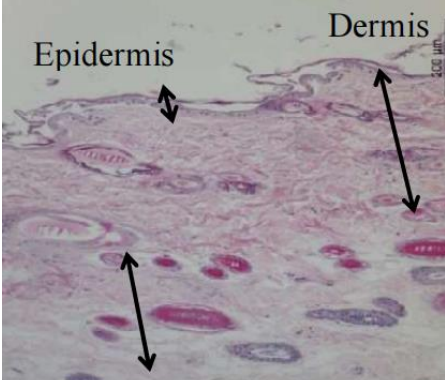
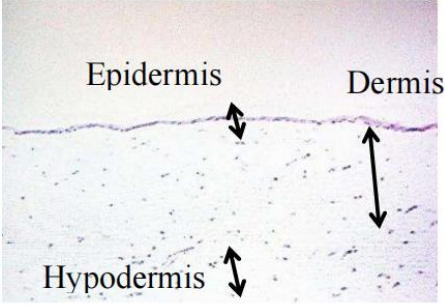
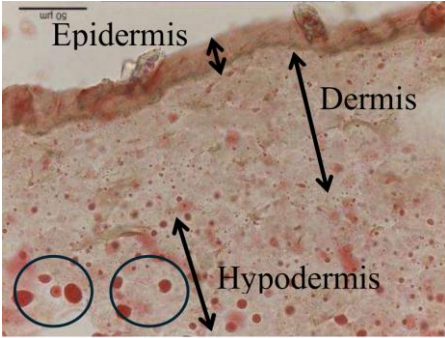
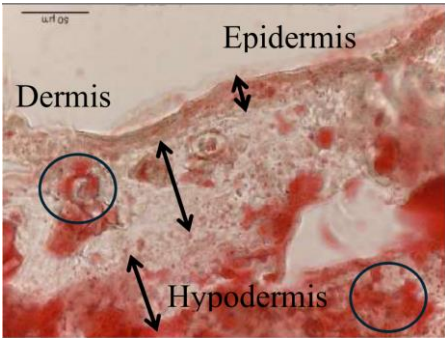
Table 7. Solubility Study of Astaxanthin in Various Medium (n=3).

No.	Solvent/Co-solvent	Average Percentage	Solubility (µg)
1	PBS: T80 (98:2)	13.255	26.5100 ± 0.0042
2	PBS: T80: EtOH (73:2:25)	11.951	23.9028 ± 0.0010
3	PBS: T80: EtOH (79:1:20)	11.629	23.2595 ± 0.0010
4	EtOH	10.953	21.9070 ± 0.0010
5	PBS: EtOH (80:20)	4.135	8.2708 ± 0.0010
6	PBS	1.580	3.1601 ± 0.0013

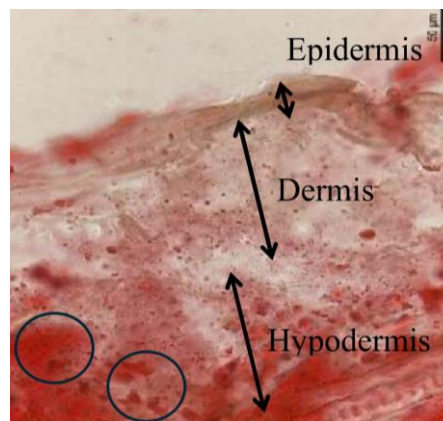
EtOH: Ethanol, PBS: Phosphate Buffer Solution pH 7.4, T80: Tween 80

*Value is expressed as Mean \pm SD

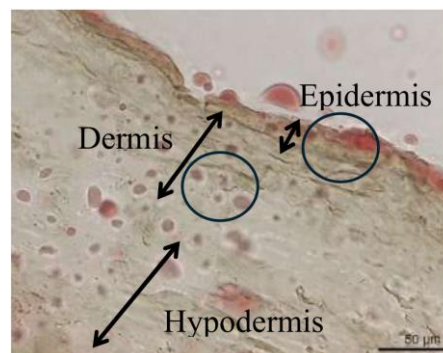
Table 8. Skin under 40X light microscope. The arrows indicate the layer, and the circles (red spots) indicate the formulation.

No.	Types	Sample
1	Skin under H&E	 <p data-bbox="1066 757 1241 790">Hypodermis</p>
2	Control ORO	
3	NE MCT oil	
4	NE Mixed oil	

5 NEG MCT oil



6 NEG Mixed oil



NE: Nanoemulsion, NEG: Nanoemulgel, MCT: Medium chain triglyceride

For the NE formulations, MCT oil NE shows higher permeation and distribution. This is evidenced by the red dots, which represent the lipid part of the formulation, being distributed into the deeper layers of the hypodermis, with only a small portion retained in the dermis layer. Conversely, the mixed oil NE indicates that the formulation is retained more in the dermis layer compared to the MCT oil formulation. The reason for better permeation in MCT oil is that the fatty acid chains in MCT oil are shorter, making it a smaller molecule compared to mixed oil NE, which allows a better transportation into the skin [34]. Both formulations permeate deeper into the skin due to their small particle sizes, resulting in less retention in the dermis and more permeation into the hypodermis.

For the NEG formulations, MCT oil shows better permeation into the hypodermis layer, with red dots more widely distributed in this region. In contrast, the mixed oil NEG shows less permeation, with red dots observed in both the epidermis and dermis layers. However, both formulations show better retention in the skin compared to NE. This may be due to the larger particle size of the NEG compared to the NE, which allows it to suspend more in the dermis layer [49].

The histology results demonstrate that MCT oil exhibits superior permeation properties compared to

mixed oil in both NE and NEG formulations. Shorter fatty acid chains of MCT oil result in smaller molecular size, facilitating deeper penetration into the dermis and hypodermis layers. The NEG formulations show better overall retention in the skin compared to NEs, which is likely due to their larger particle size that allows for prolonged suspension in the dermis layer. Although the mixed oil formulation exhibits less permeation, it demonstrates greater retention in the dermis, suggesting an extended duration of action. Therefore, MCT oil is advantageous for deeper skin permeation, while mixed oil may be beneficial for sustained dermal retention and prolonged therapeutic effects [34, 49].

CONCLUSION

In summary, while NE formulations facilitate better AST penetration into the skin compared to NEG formulations, the latter demonstrates superior properties for effective antioxidant action. This is because the NEG formulation allows the active ingredient to remain suspended in the dermis layer, where it can exert its effects more efficiently due to factors such as bigger particle size and higher stability compared to NE. Mixed oil NEG has the largest particle size that allows greater retention in the dermis and has a good PDI. However, it has lower stability due to the low

zeta potential, suggesting that it is not suitable to be kept for a long duration of time.

ACKNOWLEDGEMENTS

The author would like to thank the Ministry of Higher Education, Malaysia, for the provision of a research grant under the Fundamental Research Grant Scheme (FRGS) (FRGS/1/2021/STG04/UITM/02/8). Special thanks to the Faculty of Pharmacy, Universiti Teknologi MARA for all the resources provided throughout this project.

REFERENCES

1. Dai, X., Hu, Y., Jiang, L., Lei, L., Fu, C., Wu, S., Zhang, X., Zhu, L., Zhang, F., Chen, J., Zeng, Q. (2023) Decreased oxidative stress response and oxidant detoxification of skin during aging. *Mechanisms of Ageing and Development*, **216**, 111878.
2. Wang, X. F., Huang, Y. F., Wang, L., Xu, L. Q., Yu, X. T., Liu, Y. H., Li, C. L., Zhan, J. Y. Y., Su, Z. R., Chen, J. N., Zeng, H. F. (2016) Photo-protective activity of pogostone against UV-induced skin premature aging in mice. *Experimental Gerontology*, **77**, 76–86.
3. Nikolaidis, M. G., Margaritelis, N. V. (2023) Free radicals and antioxidants: appealing to magic. *Trends in Endocrinology & Metabolism*, **34(9)**, 503–504.
4. Dutta, S., Kumar, S. P. J., Banerjee, R. (2023) A comprehensive review on astaxanthin sources, structure, biochemistry and applications in the cosmetic industry. *Algal Research*, **74**, 103168.
5. Cyriac, F., Yi, T. X., Chow, P. S. (2023) Predicting textural attributes and frictional characteristics of topical formulations based on non-linear rheology. *Biotribology*, **35-36**, 100249.
6. Barradas, T. N., de Campos, V. E. B., Senna, J. P., Coutinho, C. dos S. C., Tebaldi, B. S., Silva, K. G. de H., Mansur, C. R. E. (2015) Development and characterization of promising o/w nano-emulsions containing sweet fennel essential oil and non-ionic surfactants. *Colloids and Surfaces A: Physicochemical and Engineering Aspects*, **480**, 214–221.
7. Mekhloufi, G., Vilamosa, N., Agnely, F. (2022) Nanoemulsion stabilized by β -lactoglobulin: A promising strategy to encapsulate curcumin for topical delivery. *Materials Today: Proceedings*, **53**, 168–173.
8. Ho, T. M., Abik, F., Mikkonen, K. S. (2022) An overview of nanoemulsion characterization via atomic force microscopy. *Critical Reviews in Food Science and Nutrition*, **62**, 4908–4928.
9. Pavoni, L., Perinelli, D. R., Ciacciarelli, A., Quassinti, L., Bramucci, M., Miano, A., Casettari, L., Cespi, M., Bonacucina, G., Palmieri, G. F. (2020) Properties and stability of nanoemulsions: How relevant is the type of surfactant? *Journal of Drug Delivery Science and Technology*, **58**, 101772.
10. Devi, S., Sangeeta, K., Beena, K. (2020) Emugel for topical drug delivery: A novel approach. *GSC Biological and Pharmaceutical Sciences*, **11(3)**, 104–114.
11. Brianna, A., Teow, S. Y., Wu, Y. S. (2023) Nanogel-based drug delivery system as a treatment modality for diverse diseases: Are we there yet? *Journal of Drug Delivery Science and Technology*, **105**, 105224.
12. Azadi, S., Osanloo, M., Zarenezhad, E., Farjam, M., Jalali, A., Ghanbariasad, A. (2023) Nano-scaled emulsion and nanogel containing *Mentha pulegium* essential oil: cytotoxicity on human melanoma cells and effects on apoptosis regulator genes. *BMC Complementary Medicine and Therapies*, **23(1)**, 1–10.
13. Goon, D. E., Abdul Kadir, S. H. S., Latip, N. A., Rahim, S. A., Mazlan, M. (2019) Palm oil in lipid-based formulations and drug delivery systems. *Biomolecules*, **9**, 134.
14. Walker, R. M., Gumus, C. E., Decker, E. A., McClements, D. J. (2017) Improvements in the formation and stability of fish oil-in-water nanoemulsions using carrier oils: MCT, thyme oil, and lemon oil. *Journal of Food Engineering*, **211**, 60–68.
15. Shibani, S., Pooja, T. (2023) Method for evaluating penetration of drug into skin. *Skin Research and Technology*, **23(3)**, 299–308.
16. Wojciechowicz, K., Gledhill, K., Ambler, C. A., Manning, C. B., Jahoda, C. A. B. (2013) Development of the mouse dermal adipose layer occurs independently of subcutaneous adipose tissue and is marked by restricted early expression of FABP4. *PLoS ONE*, **8(3)**, e59811.
17. Japir, A. A. W., Salimon, J., Derawi, D., Bahadi, M., Yusop, M. R. (2016) Purification of high free fatty acid crude palm oil using molecular distillation. *Asian Journal of Chemistry*, **28(11)**, 2549–2554.
18. Bahadi, M., Salimon, J., Derawi, D. (2022) Synthesis of ISO Grade 46 and 68 Biolubricant

- from Palm Kernel Fatty Acids. *Sains Malaysiana*, **51(8)**, 2507–2529.
19. Zhu, S., Jia, L., Wang, X., Liu, T., Qin, W., Ma, H., Lv, Y., Hu, J., Guo, Q., Tan, S., Yue, X., Yan, Y., Liu, Y., Xia, Q., Zhang, P., Zhang, H., Li, N. (2024) Anti-aging formula protects skin from oxidative stress-induced senescence through the inhibition of CXCR2 expression. *Journal of Ethnopharmacology*, **318**, 116996.
 20. Zeng, L., Zhang, Y. (2016) Impact of short-chain alcohols on the formation and stability of nano-emulsions prepared by the spontaneous emulsification method. *Colloids and Surfaces A: Physicochemical and Engineering Aspects*, **509**, 591–600.
 21. Chuo, S. C., Mohd Setapar, S. H. (2022) Application of nanoemulsion in cosmetics. *Nanotechnology for the Preparation of Cosmetics using Plant-Based Extracts*, 355–371.
 22. Tayah, D. Y., Eid, A. M. (2023) Development of miconazole nitrate nanoparticles loaded in nano-emulgel to improve its antifungal activity. *Saudi Pharmaceutical Journal*, **31(4)**, 526–534.
 23. Shnoudeh, A. J., Hamad, I., Abdo, R. W., Qadumii, L., Jaber, A. Y., Surchi, H. S., Alkelany, S. Z. (2019) Synthesis, characterization, and applications of metal nanoparticles. *Biomaterials and Bionanotechnology*, 527–612.
 24. Al Ashmawy, A. Z. G., Balata, G. F. (2024) Formulation and in vitro characterization of nanoemulsions containing remdesivir or licorice extract: A potential subcutaneous injection for coronavirus treatment. *Colloids and Surfaces B: Biointerfaces*, **234**, 113703.
 25. Khalid, N., Shu, G., Holland, B. J., Kobayashi, I., Nakajima, M., Barrow, C. J. (2017) Formulation and characterization of O/W nanoemulsions encapsulating high concentration of astaxanthin. *Food Research International*, **102**, 364–371.
 26. Ling, J., Du, Y., Sheng, Y., Wang, W., Wu, H., Chen, G., Lv, H. (2023) Influence of cryopreservation methods of ex vivo rat and pig skin on the results of in vitro permeation test. *European Journal of Pharmaceutics and Biopharmaceutics*, **189**, 109–121.
 27. Gu, L., Wang, W., Wu, B., Ji, S., Xia, Q. (2023) Preparation and in vitro characterization studies of astaxanthin-loaded nanostructured lipid carriers with antioxidant properties. *Journal of Biomaterials Applications*, **38(2)**, 292–301.
 28. Sheshala, R., Anuar, N. K., Abu Samah, N. H., Wong, T. W. (2019) In vitro drug dissolution/permeation testing of nanocarriers for skin application: A comprehensive review. *AAPS PharmSciTech*, **20**, 1–20.
 29. Ahmed, O. A. A., Badr-Eldin, S. M. (2019) Development of an optimized avanafil-loaded invasomal transdermal film: Ex vivo skin permeation and in vivo evaluation. *International Journal of Pharmaceutics*, **570**, 118657.
 30. Sundar, M., Lingakumar, K. (2023) Investigating the efficacy of topical application of Ipomoea carnea herbal cream in preventing skin damage induced by UVB radiation in a rat model. *Heliyon*, **9(9)**, e19161.
 31. Goon, D. E., Abdul Kadir, S. H. S., Latip, N. A., Rahim, S. A., Mazlan, M. (2019) Palm oil in lipid-based formulations and drug delivery systems. *Biomolecules*, **9**, 1–20.
 32. Auttajinda, N., Raviyan, P., Klangpetch, Ueno, W., Jirattananangri, W., Osiriphun, S. (2023) Antibacterial activities of palmitic and lauric acids from palm kernel oil for the development of food-grade disinfectants. *Journal of Antibacterial Studies*, **12**, 345–367.
 33. Dian, N. L. H. M., Hamid, R. A., Kanagaratnam, S., Isa, W. R. A., Hassim, N. A. M., Ismail, N. H., Omar, Z., Sahri, M. M. (2017) Palm oil and palm kernel oil: Versatile ingredients for food applications. *Journal of Oil Palm Research*, **29(4)**, 487–511.
 34. Zulfakar, M. H., Pubadi, H., Ibrahim, S. I., Hairul, N. M. (2024) Medium-chain triacylglycerols (MCTs) and their fractions in drug delivery systems: A systematic review. *Journal of Oleo Science*, **73**, 293–310.
 35. Qian, Y., Rudzińska, M., Grygier, A., Przybylski, R. (2020) Determination of triacylglycerols by HTGC-FID as a sensitive tool for the identification of rapeseed and olive oil adulteration. *Molecules*, **25(17)**, 3881.
 36. Sundaram, H., Du, A., Yatskayer, M., Lynch, S., Krol, Y., Oresajo, C. (2016) Pilot evaluation of a novel topical formulation containing high level, cholesterol-dominant, physiological lipids for specific targeting of skin barrier deficits in aging skin. *Journal of Drugs in Dermatology*, **15(12)**, 1513–1523.
 37. Nakmode, D., Bhavana, V., Thakor, P., Madan, J., Kumar Singh, P., Bala Singh, S., Rosenholm, J. M.,

- Bansal, K. K., Mehra, N. K. (2022) Fundamental aspects of lipid-based excipients in lipid-based product development. *Pharmaceutics*, **14**(4), 831.
38. Su, R., Fan, W., Yu, Q., Dong, X., Qi, J., Zhu, Q., Zhao, W., Wu, W., Chen, Z., Li, Y., Lu, Y. (2017) Size-dependent penetration of nano-emulsions into epidermis and hair follicles: implications for transdermal delivery and immunization. *Oncotarget*, **8**(24), 38214–38226.
39. Maguire, C. M., Rösslein, M., Wick, P., Prina-Mello, A. (2018) Characterisation of particles in solution—a perspective on light scattering and comparative technologies. *Science and Technology of Advanced Materials*, **19**(1), 732–745.
40. Begum, F., Chutia, H., Bora, M., Deb, P., Mahanta, C. L. (2024) Characterization of coconut milk waste nanocellulose based curcumin-enriched Pickering nanoemulsion and its application in a blended beverage of defatted coconut milk and pineapple juice. *International Journal of Biological Macromolecules*, **259**(2), 129305.
41. Danaei, M., Dehghankhold, M., Ataei, S., Hasanzadeh Davarani, F., Javanmard, R., Dokhani, A., Khorasani, S., Mozafari, M. R. (2018) Impact of particle size and polydispersity index on the clinical applications of lipidic nanocarrier systems. *Pharmaceutics*, **10**(2), 57.
42. Bahloul, B., Ben Bnina, E., Hamdi, A., Castillo Henríquez, L., Baccar, D., Kalboussi, N., Abbassi, A., Mignet, N., Flamini, G., Vega-Baudrit, J. R. (2024) Investigating the wound-healing potential of a nanoemulsion–gel formulation of *Pituranthos tortuosus* essential oil. *Gels*, **10**(3), 155.
43. Muneer, R., Hashmet, M. R., Pourafshary, P., Shakeel, M. (2023) Unlocking the power of artificial intelligence: accurate zeta potential prediction using machine learning. *Nanomaterials*, **13**(7), 1209.
44. Eid, A. M., El-Enshasy, H. A., Aziz, R., Elmarzughi, N. A. (2014) Preparation, characterization and anti-inflammatory activity of *Swietenia macrophylla* nanoemulgel. *Journal of Nanomedicine and Nanotechnology*, **5**(2), 1–10.
45. Lukić, M., Pantelić, I., Savić, S. D. (2021) Towards optimal pH of the skin and topical formulations: From the current state of the art to tailored products. *Cosmetics*, **8**(3), 69.
46. Casella, P., Iovine, A., Mehariya, S., Marino, T., Musmarra, D., Molino, A. (2020) Smart method for carotenoids characterization in *Haematococcus pluvialis* red phase and evaluation of astaxanthin thermal stability. *Antioxidants*, **9**(5), 422.
47. Camirand Lemyre, F., Chalifoux, K., Desharnais, B., Mireault, P. (2022) Squaring things up with R2: what it is and what it can (and cannot) tell you. *Journal of Analytical Toxicology*, **46**(4), 443–448.
48. Gherabli, A., Grimi, N., Lemaire, J., Vorobiev, E., Lebovka, N. (2023) Extraction of valuable biomolecules from the microalga *Haematococcus pluvialis* assisted by electrotechnologies. *Molecules*, **28**(5), 2089.
49. Izza, N., Suga, K., Okamoto, Y., Watanabe, N., Bui, T. T., Wibisono, Y., Fadila, C. R., Umakoshi, H. (2021) Systematic characterization of nano-structured lipid carriers from cetyl palmitate/caprylic triglyceride/Tween 80 mixtures in an aqueous environment. *Langmuir*, **37**(14), 4284–4293.
50. Yassin, A. E. B., Massadeh, S., Alshwaimi, A. A., Kittaneh, R. H., Omer, M. E., Ahmad, D., Aodah, A.H., Shakeel, F., Halwani, M., Alanazi, S. A., Alam, P. (2024) Tween 80-based self-assembled mixed micelles boost valsartan transdermal delivery. *Pharmaceutics*, **17**(1), 19.
51. Haan, K. D., Zhang, Y., Zuckerman, J. E., Liu, T., Sisk, A. E., Diaz, M. F. P., Jen, K. Y., Nobori, A., Liou, S., Zhang, S., Riahi, R., Rivenson, Y., Wallace, W. D., Ozcan, A. (2021) Deep learning-based transformation of H&E-stained tissues into special stains. *Nature Communications*, **12**(1), 1–13.
52. Alyoussef, A., El-Gogary, R. I., Ahmed, R. F., Ahmed Farid, O. A., Bakeer, R. M., Nasr, M. (2021) The beneficial activity of curcumin and resveratrol loaded in nanoemulgel for healing of burn-induced wounds. *Journal of Drug Delivery Science and Technology*, **62**, 102360.